Journal of Inorganic and General Chemistry
ZAAC
Zeitschrift für anorganische und allgemeine Chemie
doi.org/10.1002/zaac.202100206
ARTICLE

A Combined Theoretical and Photoelectron Spectroscopy Study of $Al_3H_n^-$ ($n = 1–9$) clusters

Jing Xu[+],[a] Xinxing Zhang[+],[b] Haopeng Wang,[b] Lijuan Fu,[a] Xiang Li,[b] Andrej Grubisic,[b] Rachel M. Harris,[b] Bryan Eichhorn,[c] Gerd Gantefoer,[b] Yihong Ding,[a] Boggavarapu Kiran,[d] Anil K. Kandalam,[e] and Kit H. Bowen*[b]

Combined photoelectron spectroscopic experiments and computational studies have been performed on $Al_3H_n^-$ ($n = 1–9$) clusters. Three modes of hydrogen bonding to the Al_3 moiety have been observed: terminal, bridging, and capping. Among various hydrides, $Al_3H_5^-$ and $Al_3H_8^-$ clusters have highest HOMO-LUMO gap and largest electron affinity, respectively. Our studies indicate that as the number of hydrogen atoms increase the presence of AlH_2 groups, representing the tetrahedral coordination of the Al atom, which in turn led to the stoichiometric ring structure.

Introduction

The hydrides of Group 13 elements, especially B and Al, have received a great attention due to their promising potential as hydrogen-storage species and high-energy density materials.[1,2] So far, boron hydrides have been extensively studied, resulting in the fruitful borane chemistry.[1,3–5] However, knowledge of the aluminum hydrides is still very limited.[2] The absence of reliable experimental data can partially be ascribed to the highly reactive bonds formed between Al and H elements, which have rendered great challenge in synthesis and characterizations. At present, only small alanes AlH_3 and Al_2H_6 have been identified in both cryogenic matrices and the gas phase.[6–8] The AlH_3 compound, which has 10.1 wt% of hydrogen and a density of 0.148 g/ml, can grow into ring or chain polymeric structures through hydrogen bridges, similar to the ways how AlH_4^-, AlH_6^{3-} and $Al_2H_7^{4-}$ aggregate in alkali metal salts.[9] Unlike the above examples where H bridges were observed, an unprecedented aluminum chain was observed in the $Li_2Al_3H_8^-$ cluster, where the $Al_3H_8^{3-}$ kernel mimics the propane molecule.[10] State-of-the-art gas phase techniques facilitate the study of these highly reactive compounds; more than two hundred new aluminum hydride cluster anions were discovered in the gas phase and characterized by anion photoelectron spectroscopy,[11–17] thus becoming a major source of the knowledge on aluminum hydrides.

Small alanes Al_mH_n ($m < 4$) are important intermediates in producing larger alanes. Yet, they don't follow the well-known Wade-Mingos rule.[1,4,18] Moreover, in these simple systems, the bonding associated with H-atoms might compete with the Al–Al bonding, different from the situation in larger alanes where the electron counting in Al_m-cluster plays an important role.[11,12,13] Therefore, despite the simplicity, the inherent bonding complexity has resulted a lot of low-lying isomers. Calculations on Al_3H_n, $n = 1$, 2, 5, 7, 9 have already been reported,[19–30] but their ground state structures are inconclusive. For example, the ground state structure of Al_3H_5 was suggested to be the consequence of adding two single H bridge to Al_3H_3,[25,26] but also considered to have a double bridge.[24,27] We should note that most of the theoretical work on Al_3H_n (except ref. 22, 25, 28–30) were carried out at the density functional theory (DFT) level with no higher-level energy corrections.

In this paper, with combined photoelectron spectroscopic experiments and DFT based computations, we carried out a systematic investigation of the structures and the bonding patterns of $Al_3H_n^-$ (n = 1–9) clusters.

Methods

Experimental

Aluminum hydrides were generated in pulsed arc cluster ionization source (PACIS),[31] which has been described in detail previously.[13] In brief, a ~30 μs long 150 V electrical pulse were applied at 10 Hz across a copper anode and an aluminum cathode of the discharging chamber vaporizing aluminum atoms and forming plasma. At the same time, ~200 psi of ultrahigh purity hydrogen gas was also introduced into the discharge region, where it was dissociated into hydrogen

[a] J. Xu,[+] L. Fu, Y. Ding
State Key Laboratory of Theoretical and Computational Chemistry, Institute of Theoretical Chemistry, Jilin University, Changchun 130023, People's Republic of China
[b] X. Zhang,[+] H. Wang, X. Li, A. Grubisic, R. M. Harris, G. Gantefoer, K. H. Bowen
Departments of Chemistry and Material Sciences, Johns Hopkins University, Baltimore, Maryland, MD 21218, USA
E-mail: kbowen@jhu.edu
[c] B. Eichhorn
Department of Chemistry, University of Maryland at College Park, College Park, MD 20742, USA
[d] B. Kiran
Department of Chemistry and Physics, McNeese State University, Lake Charles, LA 70609, USA
[e] A. K. Kandalam
Department of Physics and Engineering, West Chester University, West Chester, PA 19383, USA
[+] These authors contributed equally.

atoms. The resulting mixture of atoms, ions, and electrons then reacted and cooled as it flowed along a 20 cm tube before exiting into high vacuum. The resulting anions were then extracted and mass-selected prior to photodetachment.

Anion photoelectron spectroscopy is conducted by crossing a mass-selected beam of negative ions with a fix-frequency photon beam and energy-analyzing the resultant photodetached electrons. This process is governed by the energy-conserving relationship, $h\nu = EBE + EKE$, where $h\nu$ is the photon energy, EBE is the electron binding energy, and EKE is the electron kinetic energy. Our apparatus, which has been described in detail elsewhere,[32] consists of an ion source, a time-of-flight mass spectrometer, a Nd:YAG photodetachment laser, and a magnetic bottle photoelectron spectrometer (MB-PES). The instrumental resolution of the MB-PES is ~35 meV at 1 eV EKE. The fourth harmonic (266 nm, 4.661 eV/photon) of a Nd:YAG was used for photodetachment of anions of interest. Photoelectron spectra were calibrated against the well-known atomic lines of Cu^-.[33]

Computational

We performed isomeric search for $Al_3H_n^q$ ($q = 0, -1$; $n = 1–11$) through the "topology strategies", followed by vibrational frequency confirmation to ensure that a local minimum isomer has all real frequencies. As shown in Figure 1, the initial configurations were established based on the following considerations: i) cyclic and open Al_3-skeleton, ii) terminal (-AlH, -AlH_2) and bridge (i.e., side mono-bridge –Al(H)Al, side di-bridge –$Al(H)_2Al$, face bridge △(H)) hydrogen bonds. Note that the △(H) bond is only associated with the close structure. In this way, we totally obtained nearly three thousand initial structures. The initial geometrical optimization of various structures was performed at the B3PW91/3-21G(d) level. Excluding the structures with H_2-extrusion or Al-extrusion, the remaining structures had been optimized at the higher B3PW91/TZVP level. Finally, we obtained 285 structures with all positive frequencies, and the CCSD(T)/cc-pVTZ single-point calculations were performed on the isomers with the energy differences less than 10 kcal/mol to get reliable energetics of these alanes. For the isomers with close energies, computationally more expensive CCSD(T)/aug-cc-pVTZ (energy less than 5 kcal/mol) single-point calculations were performed to ensure the exact ground structures. The vertical electron detachment energy (VDE), the adiabatic detachment energies (ADE), and HOMO-LUMO gap were calculated at both the B3PW91/TZVP and CCSD(T)/aug-cc-pVTZ//B3PW91/TZVP levels. All calculations were carried out using Gaussian 09 program package.[34]

Results and discussion

The photoelectron spectra of $Al_3H_n^-$ ($n = 1$-9) cluster anions are presented in Figure 2. Multiple peaks (features) are observed in the spectra, except for $Al_3H_8^-$ and $Al_3H_9^-$. The position of the peaks in each spectrum measures the electron binding energies (EBE) of the photo-detachment transitions from the ground electronic state of the particular cluster anion to the ground and excited states of the neutral counterpart. The electron affinity (EA) of the neutral can be estimated from the EBE values at the onset region in the lowest EBE band in the spectrum. By definition, the EA is the energy difference between the ground states of the anion and the neutral. The calculated ADE is defined as the energy difference between the ground state structure of the anion and the neutral cluster relaxed to a local minimum near the anionic structure. If the ground state structures of anion and neutral clusters are similar, ADE and EA should be the same value. If multiple peaks are observed in the spectra, the intensity maxima of these peaks represent

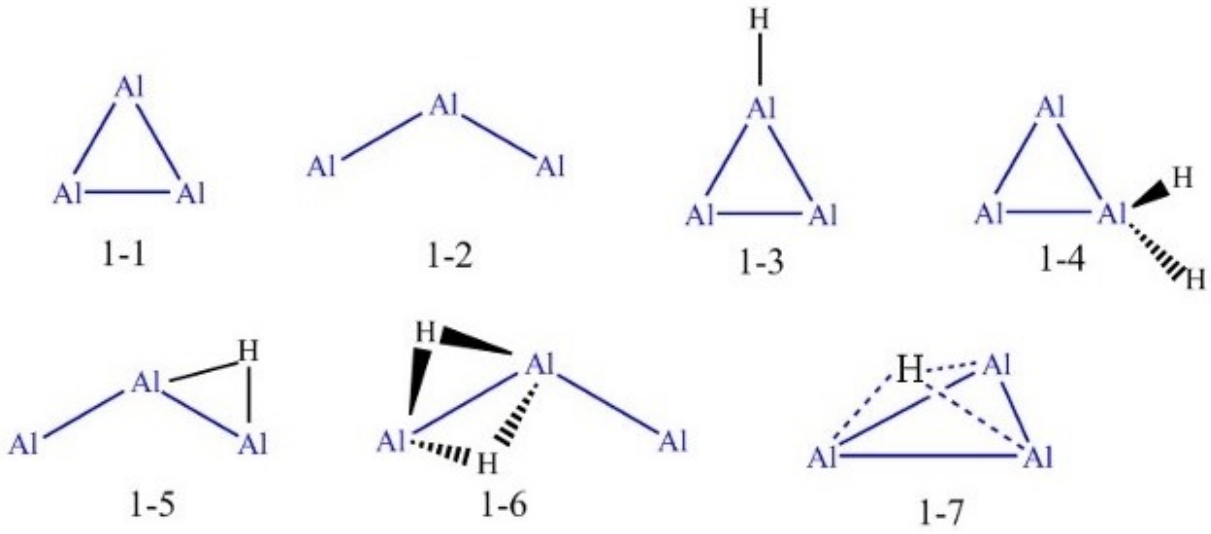

Figure 1. The initial configurations based on cyclic and open Al3-skeleton, terminal (–AlH, –AlH_2) and bridge (i.e., side mono-bridge –Al(H)Al, side di-bridge –$Al(H)_2Al$, face bridge △(H)) hydrogen bonds.

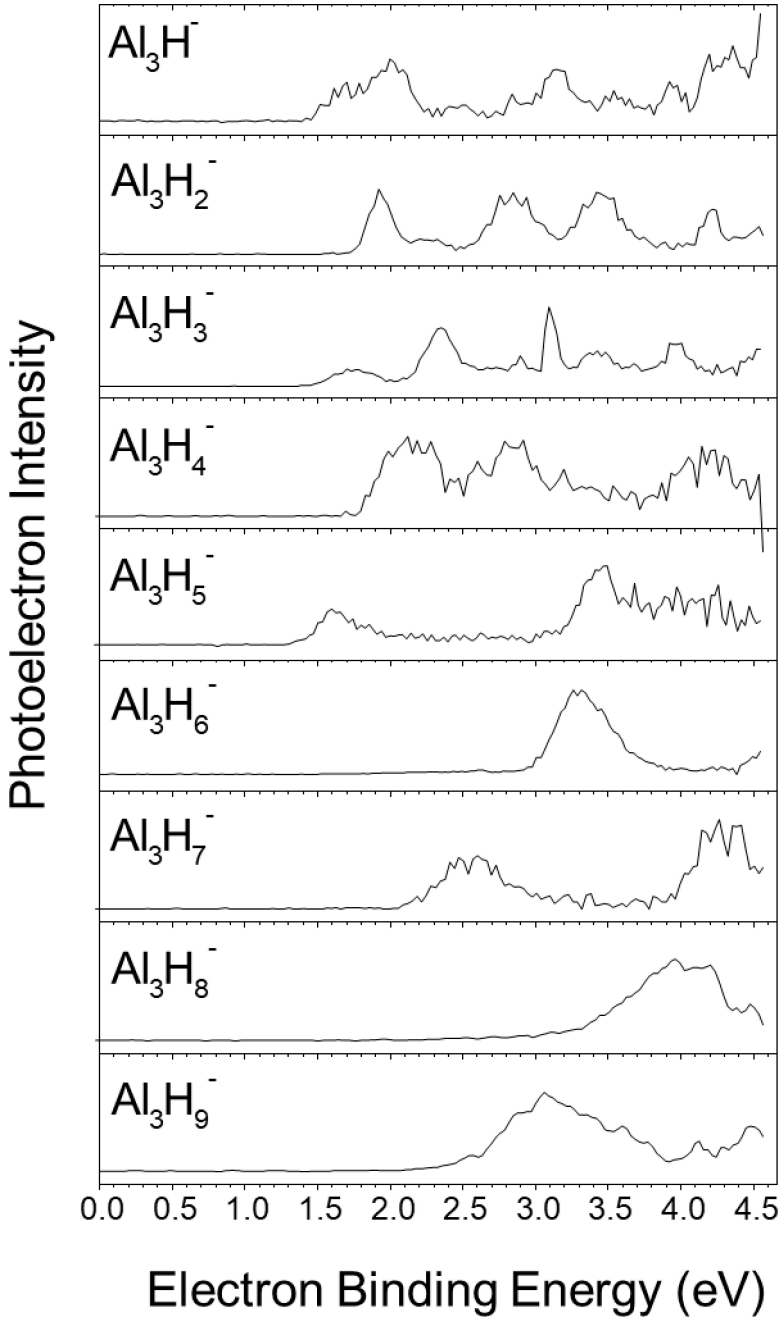

Figure 2. Photoelectron spectra of $Al_3H_n^-$ (n = 1–9) cluster anions.

transitions from the ground state of anion to the excited states of the neutral counterpart. Among these transitions, the lowest transition is the vertical detachment energy (VDE) of the anion, which is the energy difference between the ground state anion and its neutral counterpart at the geometry of the anion. Estimated EA and transition energies are listed in Table 1 for comparison with computational results. The calculated VDE and ADE values at the DFT level of theory are not only comparable to the corresponding CCSD(T) values but also at times closer to the experimental results. Therefore, we have primarily used DFT results throughout the manuscript.

To better understand the $Al_3H_n^q$ ($q = -1$; $n = 1$–9) clusters, we first focus on the bonding in the bare Al_3^- cluster. The Al_3^- forms a perfect triangle (D_{3h}) with an Al–Al bond length of 2.54 Å. The distribution of the ten valence electrons is shown as molecular orbital diagram in Figure 3. The HOMO ($2a_1'$) consists of three in plane Al 3*p* orbitals pointing towards the center. This type of σ-bonding is typical for three-membered rings observed in both $C_3H_3^+$ and C_3H_6. The next orbital, HOMO-1 ($1a_2'$) is a π-bonding orbital from the out-of-plane combination of Al 3*p* orbitals. Note that HOMO and HOMO-1 are very close in energy. The next three orbitals (1e′ and $1a_1'$), significantly lower in

Table 1. Experimentally measured VDE and ADE values and the calculated VDE and ADE values of $Al_3H_n^-$ (n = 1–9) clusters. All numbers are in eV.

System	Isomer	VDE DFT	CCSD(T)	Expt.	ADE Expt.	DFT	CCSD(T)
Al_3H	$1a^-$	1.78, 1.94, 3.28	1.58, 2.19, 4.07	1.70, 2.00, 3.14, 3.53, 3.92, 4.30	1.45	1.72	1.53
Al_3H_2	$2a^-$	1.87, 2.76, 3.33	1.90, 3.36, 5.20	1.92, 2.26, 2.85, 3.42, 4.21	1.76	1.81	1.82
Al_3H_3	$3a^-$	1.79, 2.39, 4.04	1.60, 1.87, 4.73	1.73, 2.35, 2.89, 3.09, 3.42, 3.97	1.52	1.55	1.40
	$3b^-$	1.91, 2.81, 4.35	1.76, 2.42, 5.45			1.81	1.66
Al_3H_4	$4a^-$	2.20, 2.66, 4.78	2.22, 3.31, 7.42	2.12, 2.85, 4.14	1.79	1.98	1.93
	$4b^-$	1.93, 3.06, 3.68	2.02, 4.88, 8.10			1.74	1.84
Al_3H_5	$5a^-$	1.75, 3.94, 4.15	1.60, 4.20, 7.28	1.60, 3.46, 4.07	1.39	1.56	1.40
Al_3H_6	$6a^-$	3.25, 5.08, 5.11	3.41, 5.64, 8.83	3.28	2.97	2.93	3.06
Al_3H_7	$7a^-$	2.71, 4.77, 5.47	2.61, 5.14, 8.92	2.57, 4.26	2.15	2.02	1.90
	$7b^-$	2.53, 3.96, 5.34	2.70, 4.63, 8.82			1.20	1.04
Al_3H_8	$8a^-$	3.97, 5.55, 5.74	4.07, 6.68, 9.52	4.05	3.3	3.08	3.04
	$8b^-$	3.96, 4.02, 4.04	4.05, 6.10, 8.17			2.81	2.77
Al_3H_9	$9a^-$	3.28, 6.22, 6.26	3.18, 7.01, 10.87	3.06	2.5	0.79	0.65

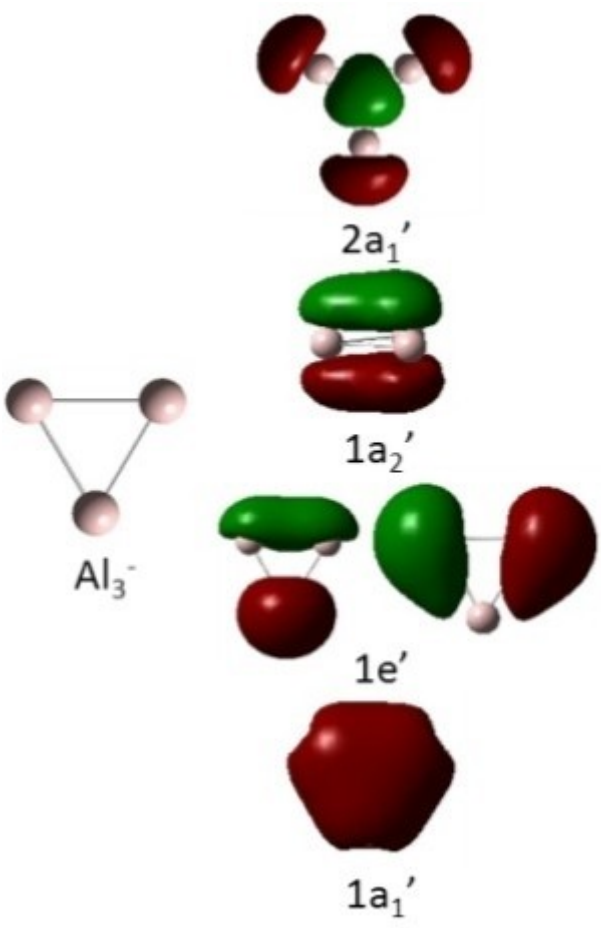

Figure 3. Molecular Orbital diagram of Al_3^-.

energy, are primarily from the Al 3 *s* orbitals with a small (< 9%) contribution from the Al 3*p*. As Wang and coworkers had observed,[35] small Al_n ($n < 5$) clusters do not have significant *s-p* hybridization, and thus in these clusters aluminum atoms essentially behave like one-electron systems. To sum up, Al_3^- is a 4-electron system, displaying both σ- (HOMO) and-π (HOMO-1) aromaticity (doubly aromatic). The double aromaticity was also observed in the La_3^- cluster.[36]

Addition of hydrogen atoms to the Al_3 can occur in at least three ways; terminal (Al–H), bridging (Al-H–Al) and capping (η^3-H). Therefore, in all of the $Al_3H_n^{-/0}$ clusters, hydrogens may adopt a combination of these bonding modes depending on the number of hydrogens and charge of the system. In the following we will discuss each $Al_3H_n^-$ cluster in detail. The calculated geometries of the two lowest energy isomers of $Al_3H_n^-$ ($n = 1$–9) are given in Figure 4, while the frontier molecular orbitals of the lowest energy isomers are shown in Figure 5.

The most stable structure of Al_3H^- is the one where hydrogen forms terminal bonding ($1a^-$) with one of the aluminum atoms, and the H-capped isomer ($1b^-$) is 0.27 eV higher in energy (Figure 4). The calculated VDE and ADE of the terminal isomer are 1.78 eV and 1.66 eV, respectively, which are in decent agreement with the corresponding experimental values of 1.70 (VDE) and 1.45 eV (EA). The calculated VDE for the capped (1.47 eV) isomer is significantly different from the experiments, indicating that only one isomer, i.e., the terminal one, has been observed in the experiments. The first vertical detachment comes from an Al–Al bonding orbital (Figure 5, 5a′). The second detachment, which is calculated to be 1.94 eV, is due to the out-of- plane pi-bonding orbital (1a′′) and matches with the experimental value of (~2.00 eV). The final detachment is from in-plane Al–Al bonding orbital (4a′) and here as well there is a good agreement between the calculations (3.28 eV) and experiments (~3.14 eV). The common bonding feature between Al_3^- and Al_3H^- is the out-of-plane pi-bonding orbital rendering them both to be pi-aromatic, however, the in-plane sigma-bonding observed in Al_3^- has been lost due to the presence of terminal H-attachment.

Adding one more hydrogen atom to Al_3H^- leads to two distinct lowest energy isomers of $Al_3H_2^-$ ($2a^-$ and $2b^-$; Figure 4). The isomer with two terminal hydrogens, $2a^-$, is more stable than $2b^-$ (one terminal and one bridge) by 0.23 eV. The

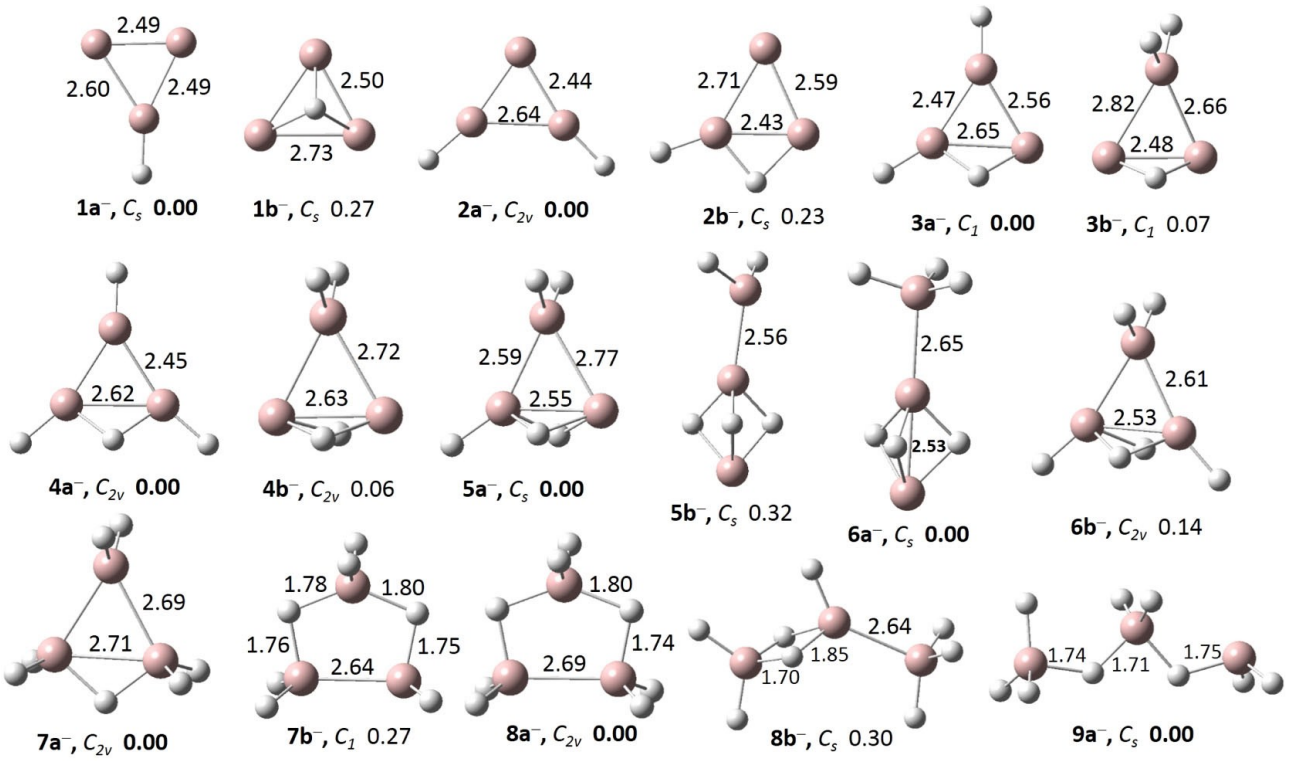

Figure 4. Calculated geometries of the two lowest energy isomers of $Al_3H_n^-$ ($n = 1$–9). The relative energies, calculated at B3PW91/TZVP level, are given in eV. All the bond lengths are given in Å.

calculated VDE/ADE values for structure $2a^-$ are 1.87/1.81 eV compares very well to the experimental values 1.92/1.76 eV. Note that the HOMO is again an out-of-plane π-bonding orbital ($1b_1$, Figure 5) similar to the one observed in both Al_3^- and Al_3H^- and all of these transitions occur around 1.80 eV. Furthermore, the measured high-energy transitions at 2.85 eV and 3.42 eV, from Al–Al bonding orbitals ($1b_2$ and $2a_1$) matches with the computed values of 2.76 eV and 3.33 eV respectively. On the other hand, the VDE (ADE) and other high-energy transitions of isomer $2b^-$ do not match with the experiments very well.

Two lowest energy isomers of $Al_3H_3^-$ ($3a^-$, and $3b^-$) are given in Figure 4. It is very hard to distinguish energetically between $3a^-$ (with two terminal and one bridging hydrogens) and $3b^-$ (with two terminal hydrogens on one aluminum atom interacting with Al-H–Al) isomers (Figure 4) as they are very close in energy (0.07 eV). Comparison of the calculated VDE (ADE) of isomer $3a^-$ 1.79 (1.55) eV and isomer $3b^-$ 1.91 (1.81) eV with experimental values of 1.73 (1.52) eV indicate that the electron detachment energies of both isomers are in good agreement with the experiments, and it is possible that both isomers are present in the cluster beam. In addition, the high-energy transitions for $3a^-$ (2.39 eV and 4.04 eV) and $3b^-$ (2.81 eV) are also in good agreement with the experiments (Table I), further confirming the presence of two isomers. The HOMO and HOMO-2 of $3a^-$ (7a and 5a, Figure 5) are a combination of Al–Al and Al–H bonding. The HOMO-1 which is a π-bonding (6a) orbital between Al atoms is significantly distorted due to the out-of plane Al-H–Al bridging. The $3b^-$ isomer can be viewed as a 1e-AlH_2 group, which is isoelectronic to hydrogen atom, interacting with AlHAl group. This structural motif is going to be the dominant unit for higher stoichiometry.

The two lowest energy isomers of $Al_3H_4^-$, $4a^-$ and $4b^-$ which have markedly different arrangement of hydrogen atoms also found to be isoenergetic (0.06 eV). The calculated VDE/ADE of $4a^-$ and $4b^-$ are 2.20/1.98 eV and 1.93/1.74 eV, respectively. The corresponding experimental numbers are 2.12/1.79 eV, which match well with the calculation. In addition, the higher transition energies from $4a^-$ ($4b^-$) and are 2.66 (3.06) and 4.71 (3.68) eV, respectively, and also match the experiments (2.85, 4.14 eV). Therefore, both isomers are present in the experiments. It is noteworthy here that the energy gap between HOMO and HOMO-1 of $4a^-$ and $4b^-$ is 1.80 eV and 0.63 eV, respectively. This significant difference can be understood from the nature of bonding in these clusters. The HOMO (5a′, Figure 5) of $4a^-$ is a distorted π-bonding-orbital akin to the one observed for $3a^-$ which is followed by an Al–Al bonding orbital (2a″). Since both are bonding orbitals their energy difference is relatively small (0.57 eV). On the other hand, the HOMO ($4a_1$, Figure 5) of $4b^-$ is a lone pair orbital on aluminum atoms followed by a bonding orbital between AlH_2 and Al-$(H)_2$-Al unit ($3a_1$, Figure 5). As a result, the energy difference between these two orbitals is quite large (1.80 eV).

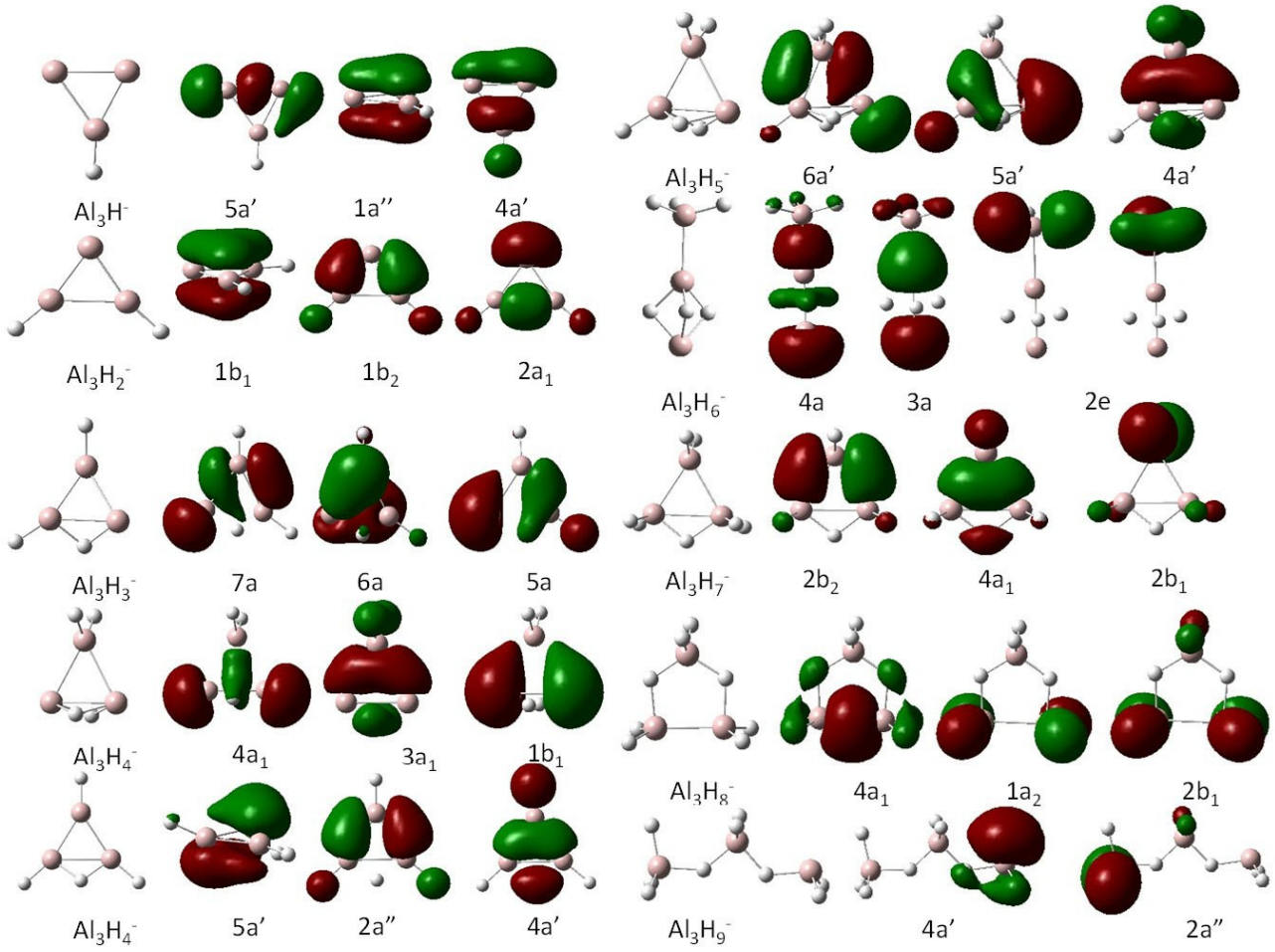

Figure 5. Selected Molecular Orbital picture of $Al_3H_n^-$ (n = 1-9).

The photoelectron spectrum of $Al_3H_5^-$ is unique among $Al_3H_n^-$ species as the spectra shows largest HOMO-LUMO gap (1.86 eV). The two lowest energy isomers are given in Figure 4. The most stable isomer, $5a^-$ is the one where one AlH_2 group interacting with HAl-$(H)_2$-Al and the second isomer, $5b^-$, which is 0.32 eV higher in energy has a linear arrangement of aluminum atoms in which two hydrogen atoms make terminal bonds with the edge aluminum and a triple hydrogen bridge between the remaining two Al atoms. The calculated VDE/ADE of $5a^-$ (1.75/1.56 eV) and $5b^-$ (1.96/1.71 eV). Hence, only the VDE/ADE values of $5a^-$ are in good agreement with the experimentally determined value (1.60/1.39 eV). The high HOMO-LUMO gap in $5a^-$ can be understood as following: bridged AlH_2 is a one-electron donor isoelectronic to H atom and the AlH group is a two-electron donor and Al atom is one electron donor. This leaves total number of available electrons '6', which forms *three* '3*c*–2*e*' bonds as Al-H–Al, making the whole cluster electron-sufficient and hence large HOMO-LUMO gap.

Similar bonding features are also responsible for the observation of second highest electron affinity for $Al_3H_6^-$. Among the two lowest energy clusters, $6a^-$ and $6b^-$ given in Figure 4, the calculated VDE/ADE of $6a^-$ (3.25/2.93 eV) are in excellent agreement with the experiments (3.28/2.97 eV). On the other hand, the VDE/ADE values of $6b^-$ (2.64/2.2 eV) are not in agreement with the experimental values. Hence, we conclude that only isomer $6a^-$ exists in the cluster beam. The bonding in $6a^-$ is very similar to $5a^-$ where bridging AlH_2 is replaced by H and the terminal H is replaced by AlH_3^- resulting in '6' electrons to from three '3*c*–2*e*' Al-H–Al bonds. As a result, the first electron transition from $6a^-$ and second transition for $5b^-$ (~ 3.30 eV) occur nearly at the same energy, providing further proof to the electronic structure.

As the number of hydrogens increases the occurrence of AlH_2 groups, which helps to form tetrahedral coordination, also increases. The two lowest energy isomers of $Al_3H_7^-$ are given in Figure 4 as $7a^-$ and $7b^-$. The calculated VDE/ADE of $7a^-$ (2.71/2.23 eV) and $7b^-$ (2.53/2.00 eV) matches with the experimental values (2.57/2.15 eV). Therefore, we conclude that both isomers are present in the cluster beam.

$Al_3H_8^-$ is also unique among the $Al_3H_n^-$ clusters in the current study. The observed VDE/EA (4.05/3.3 eV) are largest in the series for $Al_3H_8^-$. Two lowest energy structures of $Al_3H_8^-$, $8a^-$ and $8b^-$ are given in Figure 4. The calculated VDE/ADE of

$8a^-$ (3.97/3.08 eV) and $8b^-$ (3.96/2.81 eV) are in agreement with the experimental value (4.05/3.3 eV). Since the VDE and ADE values of both these isomers are in agreement with the measured values, we cannot rule out the possibility of both these isomers contributing towards the photoelectron spectrum. In isomer $8a^-$, each AlH_2 group and H atom provides 1*e*, which gives total of six valence electrons including one negative charge. This leads to two Al-H–Al '3*c*–2*e*' bonds and one Al–Al bond making the system electron sufficient. As a result, the electron affinity of isomer $8a^-$ is very high. On the other hand, isomer $8b^-$ achieves high electron affinity in a different way. Isomer $8b^-$ can be considered as a derivative of well-known Al_2H_6 with one terminal H is replaced by AlH_3^-, resulting in very stable structure. Finally, the most stable structure of $Al_3H_9^-$ (isomer $9a^-$) is shown in Figure 4. As expected, and in accordance with our earlier studies,[14] isomer $9a^-$ is a linear structure where two Al atoms form tetrahedral coordination, and each Al atom is connected through hydrogen bridges. The calculated VDE of 3.24 eV is in agreement with the experimental value of 3.06 eV.

There are no new structural motifs or new bonding patterns observed in the neutral Al_3H_n clusters. As anticipated several isomers are close in energy as the energy difference between Al-H_b and Al-H_t are similar, unless of course aided by strong electronic structural effects. Hence, the neutral clusters are not discussed here.

To understand the energetics involved in the addition of hydrogens we have considered two equations:

$$Al_3^q + (n/2)H_2 = Al_3H_n^q \quad (1)$$

$$Al_3H_n^q + (1/2)H_2 = Al_3H_{n+1}^q \quad (2)$$

in both cases *q* (charge) is either 0 or −1 and *n* is from 1 to 11

The first equation estimates the energy released by the simultaneous addition of '*n*' number of hydrogens to the Al_3 cluster. The calculated values for $n=1$ to 11 is shown in the Figure 6. Obviously, all energies are exothermic. The energy values also show strong even-odd oscillations, which get more pronounced as *n* increases. Interestingly, there is a strong drop in exothermicity on going from $n=9$ to 10 for neutral and $n=$ 10 to 11 for anion. These trends are consistent with the fact the for neutral systems $n=9$, Al_3H_9 is stochiometric unit and very stable. Addition of hydrogen is not expected to be stable. Similarly for the anion, $Al_3H_{10}^-$, which is formed by the addition of H^- to the stochiometric Al_3H_9, is most stable. Equation 2, on the other hand, describes the energy released by successive addition of hydrogens. This equation provides an opportunity

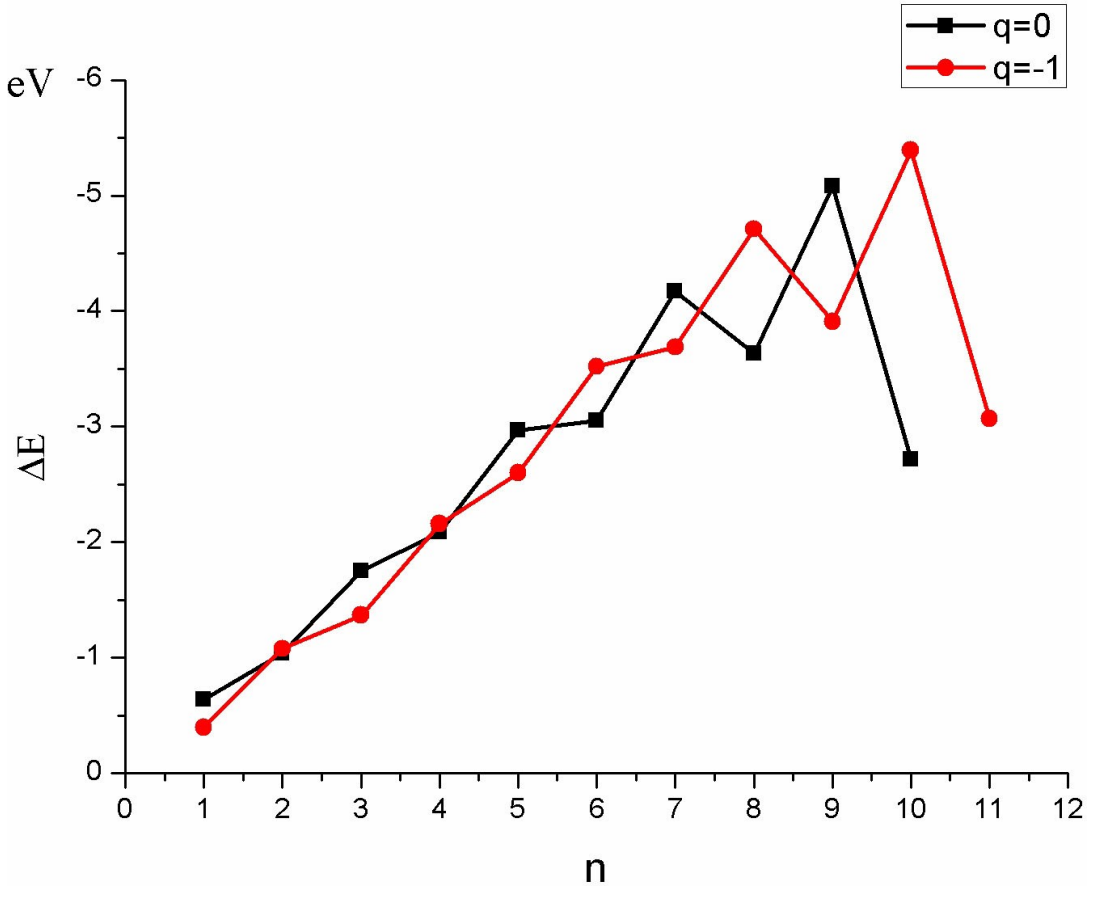

Figure 6. The variation in the amount of energy released due to simultaneous addition of "*n*" number of hydrogen atoms to an Al_3 moiety as the value of *n* increases from 1 to 11.

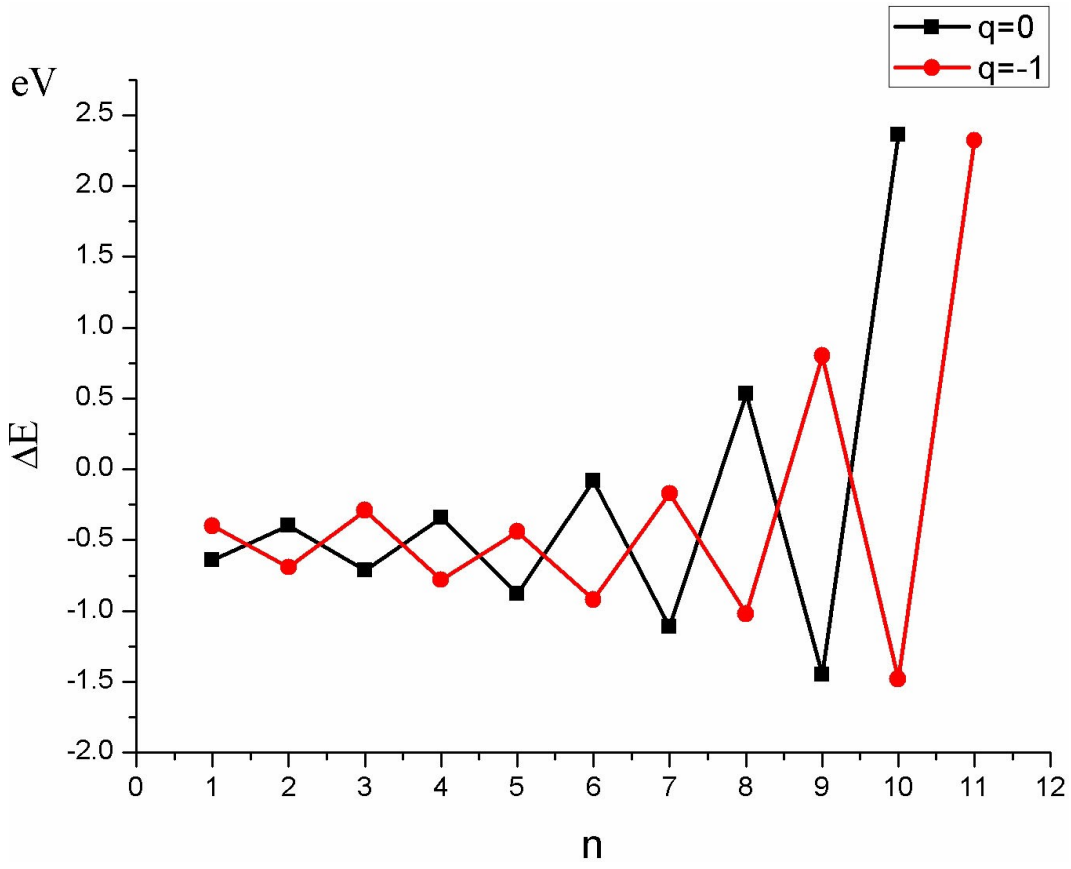

Figure 7. The variation in the amount of energy released due to *successive* addition of hydrogen atoms to an Al_3H_n cluster as the value of *n* increases from 1 to 11.

to unmask stable structures. Once again, the odd-even trend is more pronounced at larger *n* and shows enhanced stability for $n = 9$ neutral and $n = 10$ for anion as shown in Figure 7.

Concluding remarks

In conclusion, a systematic anion photoelectron spectroscopy and density functional theory-based study on $Al_3H_n^-$ ($n = 1–9$) clusters has revealed that the hydrogen atoms attach in three different bonding modes and exothermically to the aluminum clusters. Among the $Al_3H_n^-$ ($n = 1–9$) clusters, $Al_3H_8^-$ was observed to have the largest VDE and ADE values. Energetics and bonding analysis have revealed that two isomers exist for this cluster and both of them attain their unusually large electron affinity values in two different ways. Our calculated results have also shown that as the number of hydrogens increases the coordination around the aluminum atoms tend towards tetrahedral geometries.

Acknowledgments

This work was funded by the National Basic Research Program of China (973 Program) (2012CB932800), the National Natural Science Foundation of China (No. 21473069,21273093). The experimental part of this material was supported by the Air Force Office of Scientific Research (AFOSR), under Grant No. FA9550-19-1-0077 (K.H.B.).

Conflict of Interest

The authors declare no conflict of interest.

[1] R. E. Williams, *Chem. Rev.* **1992**, *92*, 177.
[2] S. Aldridge, A. J. Downs, *Chem. Rev.* **2001**, *101*, 3305.
[3] W. N. Lipscomb, *Boron Hydrides*; Benjamin Inc.: New York, **1963**.
[4] K. Wade, *Adv. Inorg. Chem. Radiochem.* **1976**, *18*, 1.
[5] A. Earnshaw, N. Greenwood, *Chemistry of the Elements*; 2nd ed.; Elsevier: The Netherlands, **1997**.
[6] P. Breisacher, B. Siegel, *J. Am. Chem. Soc.* **1964**, *86*, 2.
[7] F. A. Kurth, R. A. Eberlein, H. Schnockel, A. J. Downs, C. R. Pulham, *J. Chem. Soc. Chem. Commun.* **1993**, 1302.
[8] L. Andrews, X. F. Wang, *Science* **2003**, *299*, 2049.

[9] F. A. Cotton, G. Wilkinson, *Advanced Inorganic Chemistry: A Comprehensive Text*; 2nd ed.; Interscience Publisher: New York, **1966**.
[10] I. A. Popov, X. Zhang, B. W. Eichhorn, A. I. Boldyrev, K. H. Bowen, *Phys. Chem. Chem. Phys.* **2015**, *17*, 26079.
[11] A. Grubisic, X. Li, S. T. Stokes, J. Cordes, G. F. Gantefoer, K. H. Bowen, B. Kiran, P. Jena, R. Burgert, H. Schnoeckel, *J. Am. Chem. Soc.* **2007**, *129*, 5969.
[12] B. Kiran, P. Jena, X. Li, A. Grubisic, S. T. Stokes, G. F. Gantefoer, K. H. Bowen, R. Burgert, H. Schnoeckel, *Phys. Rev. Lett.* **2007**, 98.
[13] X. Li, A. Grubisic, S. T. Stokes, J. Cordes, G. F. Gantefoer, K. H. Bowen, B. Kiran, M. Willis, P. Jena, R. Burgert, H. Schnoeckel, *Science* **2007**, *315*, 356.
[14] X. Li, A. Grubisic, K. H. Bowen, A. K. Kandalam, B. Kiran, G. F. Gantefoer, P. Jena, *J. Chem. Phys.* **2010**, *132*, 241103.
[15] X. Zhang, H. Wang, E. Collins, A. Lim, G. Gantefoer, B. Kiran, H. Schnoeckel, B. Eichhorn, K. Bowen, *J. Chem. Phys.* **2013**, *138*, 124303.
[16] H. Wang, X. Zhang, Y. Ko, G. F. Gantefor, K. H. Bowen, X. Li, K. Boggavarapu, A. K. Kandalam, *J. Chem. Phys.* **2014**, *140*, 164317.
[17] J. D. Graham, A. M. Buytendyk, X. Zhang, E. L. Collins, K. Boggavarapu, G. Gantefoer, B. W. Eichhorn, G. L. Gutsev, S. Behera, P. Jena, K. H. Bowen, *J. Phys. Chem. A* **2014**, *118*, 8158.
[18] D. M. P. Mingos, *Nat.-Phys. Sci.* **1972**, *236*, 99.
[19] B. J. Duke, C. X. Liang, H. F. Schaefer, *J. Am. Chem. Soc.* **1991**, *113*, 2884.
[20] M. L. McKee, *J. Phys. Chem.* **1991**, *95*, 6519.
[21] N. Gonzales, J. Simons, *J. Chem. Phys.* **1994**, *101*, 10746.
[22] J. Moc, *Eur. Phys. J. D* **2007**, *45*, 247.
[23] Z. J. Li, J. H. Li, *Solid State Commun.* **2009**, *149*, 375.
[24] C. P. Nold, J. D. Head, *J. Phys. Chem. A* **2012**, *116*, 4348.
[25] D. Mallick, P. Parameswaran, E. D. Jemmis, *J. Phys. Chem. A* **2008**, *112*, 13080.
[26] G. N. Srinivas, A. Anoop, E. D. Jemmis, T. P. Hamilton, K. Lammertsma, J. Leszczynski, H. F. Schaefer III, *J. Am. Chem. Soc.* **2003**, 125, 16397.
[27] Y. H. Cui, J. G. Wang, W. Xu, *Nanotechnology* **2010**, *21*, 025702.
[28] J. Moc, K. Bober, K. Mierzwicki, *Chem. Phys.* **2006**, *327*, 247.
[29] I. Pina, G. J. Kroes, M. C. van Hemert, *J. Chem. Phys.* **2010**, *133*, 184304.
[30] L. J. Fu, C. B. Shao, L. Jin, Y. H. Ding, *Mol. Phys.* **2010**, *108*, 1715.
[31] X. Zhang, Y. Wang, H. Wang, A. Lim, G. Ganteför, K. H. Bowen, J. U. Reveles, S. N. Khanna, *J. Am. Chem. Soc.* **2013**, *135*, 4856.
[32] M. Gerhards, O. C. Thomas, J. M. Nilles, W. J. Zheng, K. H. Bowen, *J. Chem. Phys.* **2002**, *116*, 10247.
[33] J. Ho, K. M. Ervin, W. C. Lineberger, *J. Chem. Phys.* **1990**, *93*, 6987.
[34] M. J. Frisch, G. W. Trucks, H. B. Schlegel, et al., GAUSSIAN09, Revision B.01, Gaussian, Inc., Wallingford, CT, **2004**.
[35] X. Li, H. B. Wu, X. B. Wang, L. S. Wang, *Phys. Rev. Lett.* **1998**, *81*, 1909.
[36] A. Ivanov, X. Zhang, H. Wang, A. I. Boldyrev, G. Gantefoer, K. H. Bowen, I. Černušák, *J. Phys. Chem. A.* **2015**, DOI: 10.1021/acs.jpca.5b08076.

Manuscript received: June 13, 2021
Revised manuscript received: August 9, 2021
Accepted manuscript online: August 15, 2021

ARTICLE